

DETECTING THE WARM-HOT INTERGALACTIC MEDIUM THROUGH X-RAY ABSORPTION LINES

YANGSEN YAO¹, J. MICHAEL SHULL¹, Q. DANIEL WANG², AND WEBSTER CASH¹

Accepted for publication in *ApJ*

ABSTRACT

The warm-hot intergalactic medium (WHIM) at temperatures $10^5 - 10^7$ K is believed to contain 30-50% of the baryons in the local universe. However, all current X-ray detections of the WHIM at redshifts $z > 0$ are of low statistical significance ($\lesssim 3\sigma$) and/or controversial. In this work, we aim to establish the detection limits of current X-ray observatories and explore requirements for next-generation X-ray telescopes for studying the WHIM through X-ray absorption lines. We analyze all available grating observations of Mrk 421 and obtain spectra with signal-to-noise ratio (S/N) of ~ 90 and 190 per 50 mÅ spectral bin from *Chandra* and *XMM-Newton* observations, respectively. Although these spectra are two of the best ever collected with *Chandra* and *XMM-Newton*, we cannot confirm the two WHIM systems reported by Nicastro et al. in 2005. Our bootstrap simulations indicate that spectra with such high S/N cannot constrain the WHIM with O VII column densities $N_{\text{OVII}} \approx 10^{15} \text{ cm}^{-2}$ (corresponding to an equivalent widths of 2.5 mÅ for a Doppler velocity of 50 km s^{-1}) at $\gtrsim 3\sigma$ significance level. The simulation results also suggest that it would take > 60 Ms for *Chandra* and 140 Ms for *XMM-Newton* to measure the N_{OVII} at $\geq 4\sigma$ from a spectrum of a background QSO with flux of ~ 0.2 mCrab ($1 \text{ Crab} = 2 \times 10^{-8} \text{ erg s}^{-1} \text{ cm}^{-2}$ at $0.5\text{-}2 \text{ keV}$). Future X-ray spectrographs need to be equipped with spectral resolution $R \sim 4000$ and effective area $A \geq 100 \text{ cm}^2$ to accomplish the similar constraints with an exposure time of ~ 2 Ms and would require ~ 11 Ms to survey the 15 QSOs with flux $\gtrsim 0.2$ mCrab along which clear intergalactic O VI absorbers have been detected.

Subject headings: intergalactic medium — X-rays: diffuse background — quasars: absorption lines — BL Lacertae objects: individual (Markarian 421)

1. INTRODUCTION

Identifying the “missing baryons” is one of the major tasks of modern cosmology. Observations of the microwave background (e.g., Komatsu et al. 2011) and the big bang nucleosynthesis model combined with the measurement of deuterium abundance (e.g., Burles et al. 2001; O’Meara et al. 2006; Pettini et al. 2008) are converging on the cosmological baryon density of $\Omega_b = 0.0455 \pm 0.0028$. At high redshift ($z > 3$) universe, baryons exist primarily in the form of cool, photoionized intergalactic medium (IGM) that is traced by Ly α absorption forest lines (Rauch et al. 1997). In the present-day universe, matter detected in forms of photoionized IGM, stars, galaxies, intracluster medium, etc., adds up to only $\sim 50\%$ of the baryons (Shull et al. 2011), leaving much of the inventory yet to be found (Fukugita et al. 1998; Fukugita & Peebles 2004). Cosmological numerical simulations for large-structure formation indicate that the missing baryons are still in the IGM, but at current epoch they have been heated by gravitational shocks and galactic feedback to temperatures of $10^5 - 10^7$ K when they fall into the gravitational potential wells of the dark matter cosmic web filaments (e.g., Cen & Ostriker 1999, 2006; Davé et al. 2001). The IGM at these temperatures, so-called warm-hot intergalactic medium (WHIM), mainly absorbs and emits photons in the ultraviolet (UV) and X-ray wavelength bands.

Searching for the missing baryons has been conducted extensively in the UV band. Indeed, besides the cool phase Ly α absorbers (e.g., Weymann et al. 1998; Penton et al. 2000,

2004), the absorption lines of C III, C IV, N V, O VI, Si III, and Si IV have been routinely observed in spectra of background quasi-stellar objects (QSOs; e.g., Tripp et al. 2000, 2008; Prochaska et al. 2004; Lehner et al. 2006; Danforth & Shull 2005, 2008; Danforth et al. 2006; Thom & Chen 2008; Yao et al. 2011), suggesting that a significant amount of baryons exist in the highly ionized absorbers. These high ions, O VI in particular, are believed to trace the WHIM at the low-temperature end ($\sim 10^5 - 10^6$ K). However, all these ions can also be produced through photoionization in the intergalactic environment (Oppenheimer & Davé 2009; but see also Tepper-García et al. 2011 and Smith et al. 2012 for a contrary view) and thus some of them may not contribute to the canonical WHIM (i.e., the shock-heated IGM expected from simulations). How many of these absorbers originate in the real WHIM is still under debate (Danforth & Shull 2008; Tripp et al. 2008). Ne VIII and broad H I Ly α absorbers (BLAs) are complementary and valuable tracers of hot absorbing WHIM in UV bands. However, there are only a few detections with marginal significance of Ne VIII (Savage et al. 2005; Narayanan et al. 2009, 2011) and detections of BLAs require very high signal-to-noise-ratio (S/N) of spectra to resolve broad and weak signals from the continua (Richter et al. 2006; Lehner et al. 2007; Savage et al. 2011; Danforth et al. 2010, 2011). Converting measurement of these UV absorbers to census of baryonic matter also depends on ionization fractions and metallicity of the IGM, which in many absorbers are still poorly known. Nevertheless, BLAs and O VI-absorbers, although partially overlapped with photoionized Ly α absorbers, are estimated to contribute an additional $\sim 25\%$ to the baryon inventory at the current epoch (e.g., Danforth & Shull 2008; Danforth et al. 2011; Shull et al. 2011).

X-ray observations of the intergalactic O VII and O VIII emission/absorption features could provide essential informa-

¹ Center for Astrophysics and Space Astronomy, Department of Astrophysical and Planetary Sciences, University of Colorado, 389 UCB, Boulder, CO 80309; yaos@colorado.edu

² Department of Astronomy, University of Massachusetts, Amherst, MA 01003

tion for establishing the existence of the WHIM and completing the baryon inventory in the local universe. At temperatures $T \gtrsim 10^6$ K, hydrogen and helium are nearly completely ionized (Gnat & Sternberg 2007). Without metals, the thermal gas emits/absorbs photons through bremsstrahlung, which unfortunately is optically thin even at intergalactic scales (Bregman 2007). Because the K-shell transitions of all elements heavier than lithium and the L-shell transitions of elements heavier than iron lie in X-ray bands (Paerels & Kahn 2003), metals can greatly increase the emissivity of the gas. However, because of the density-squared dependence, the WHIM emission is expected to be weak and difficult to detect. In fact, the IGM emission has been directly observed only from the dense regions like intracluster and intragroup media (e.g., Wang et al. 1997; Mulchaey 2000; Allen et al. 2002; Sun et al. 2009). The WHIM emission signals were also claimed in the angular correlation of the diffuse X-ray background (Softan et al. 1999; Ursino & Galeazzi 2006), but disentangling the real WHIM signal from the unresolved point sources and local Galactic hot diffuse gas has been a major uncertainty (e.g., Galeazzi et al. 2007).

Unlike emission lines, absorption lines measure the column densities and thus directly sample the total mass of the intervening gas along a line of sight. Oxygen is the most abundant metal element. In contrast of O VI as a minority ionization state, O VII is the most abundant ion for a gas at temperatures of $T \sim 10^{5.5} - 10^{6.3}$ K and O VIII takes over when $T \gtrsim 10^{6.3}$ K (Gnat & Sternberg 2007). Thus they have advantages over O VI in estimating the total baryon contained in highly ionized absorbers. O VII and O VIII, whose production ionization potentials are 138.1 eV and 739.3 eV compared to 113.9 eV of O VI, are also hard to produce through photoionization in the IGM environment (e.g., Cen & Fang 2006; Chen et al. 2003). Theoretical calculations indicate that the O VII column density is about 10 times higher than O VI in a shock-heated gas (i.e., $N_{\text{OVII}} \gtrsim 10 N_{\text{OVI}}$) whereas $N_{\text{OVII}} \lesssim 3 N_{\text{OVI}}$ in a photoionized gas (Furlanetto et al. 2005). Therefore observations of the IGM O VII and O VIII absorption lines are crucial, not only for constraining the properties of the WHIM at high temperature end but also for probing the nature of the commonly observed O VI-absorbers.

Unfortunately, most attempts at searching the X-ray WHIM absorption lines have been frustrated. O VII and O VIII absorption lines at $z = 0$ have been unambiguously detected in many background QSOs. However, all these X-ray absorptions are *inconsistent* with an intergalactic origin (Fang et al. 2006; Bregman & Lloyd-Davies 2007; Yao et al. 2010), but rather can be attributed to the Galactic diffuse hot gas (e.g., Yao & Wang 2005, 2007; Yao et al. 2008, 2009; Wang et al. 2005). Perhaps the most compelling intergalactic result is the detection of O VII absorption at the redshift of the large galaxy structure Sculptor Wall ($z_{\text{abs}} = 0.03$) along the QSO sight line H 2356-309 ($z_{\text{QSO}} = 0.165$), albeit of low significance ($\sim 3\sigma$; Buote et al. 2009; Fang et al. 2010). However, because of the high number density of galaxies along the sight line, the absorption may sample the halo gas of one or more intervening galaxies with small impact distances ($\lesssim 50$ kpc; Williams et al. 2010), i.e., mimicking the O VII and O VIII absorption lines at $z = 0$. Therefore, it may not be representative of the typical WHIM. Furthermore, attempts at searching for the similar absorption features at the redshift of another large structure, Pisces-Cetus along the same sight line, failed (Zappacosta et al. 2010). All other claimed WHIM O VII and

O VIII absorptions have been highly debated. For instance, the detected O VIII absorption line at $z = 0.0554$ in *Chandra* spectrum of PKS 2155-304 (Fang et al. 2002a, 2007) cannot be confirmed by the *XMM-Newton* observations (Cagnoni et al. 2004), although at nearby redshift a small galaxy group and the corresponding UV O VI and Ly α absorption lines have been identified (Shull et al. 1998, 2003). Nicastro et al. (2005) obtained a spectrum with unprecedented S/N during the burst states of Mrk 421 and reported two WHIM detections at $z = 0.011$ and $z = 0.027$. Again, observations with *XMM-Newton* cannot confirm the detections and reported significances have also been questioned (Kaastra et al. 2006; Rasmussen et al. 2007). Williams et al. (2010) recently found a galaxy filament at $z = 0.027$, which makes the reported O VII WHIM detections along the Mrk 421 sight line back to be a subject of discussions.

In this work, we aim to provide detection limits of current X-ray observatories, *Chandra* and *XMM-Newton*, in measuring the WHIM through X-ray absorption lines, and establish requirements (e.g., effective area and spectral resolution) for next-generation X-ray telescopes. We begin our investigation by scrutinizing the controversial WHIM detections along the Mrk 421 sight line. We extensively explore all the available *Chandra* and *XMM-Newton* observations, and then run bootstrap simulations to test the reliability of any absorption feature.

The paper is organized as follows. In Section 2 we describe the observations and our data reduction processes, and in Section 3 we report the data analysis results and compare them with previous work. In Section 4, we run bootstrap simulations to explore the detection limits of *Chandra* and *XMM-Newton* and to establish requirements of next-generation X-ray telescopes. We summarize our results in Section 5.

Throughout the paper, we adopt the atomic data from Verner et al. (1996) and solar abundances from Asplund et al. (2009). We conduct our data analysis within *XSPEC* (version 12.6; Arnaud 1996), and report the 1σ confidence range or 3σ limit for a fitting parameter. We take the flux normalization of 1 Crab = 2×10^{-8} erg s $^{-1}$ cm $^{-2}$ at 0.5-2.0 keV. Thus 0.2 mCrab is 2.15×10^{-13} erg s $^{-1}$ cm $^{-2}$ Å $^{-1}$ for a flat spectrum in wavelength space, which corresponds to 2.34×10^{-4} photons s $^{-1}$ cm $^{-2}$ Å $^{-1}$ around the O VII K α (21.602 Å) at the rest-frame. We define measurement significance level (SL) of an absorption line as

$$SL = \frac{EW}{\Delta EW}, \quad (1)$$

where EW and ΔEW are the equivalent width and its 1σ uncertainty for an absorption line.

2. OBSERVATIONS AND DATA REDUCTION

We used all grating observations of Mrk 421 observed with both *Chandra* and *XMM-Newton* that are available as of 2011 April. Since Mrk 421 is a calibration source for both observatories, observations were taken on a nearly regular basis. The *Chandra* data were downloaded from the CXO archive web site³, which included 26 observations taken with the low energy transmission grating (LETG; ObsIDs of 1715, 4148, 4149, 5171, 5318, 5331, 5332, 6925, 8378, 8396, 10664, 10665, 10667, 10668, 10669, 10671, 11605, 11606, 11607, 11966, 11970, 11972, 11974, 12121, 12122, and 13097) with

³ <http://cda.harvard.edu/chaser/mainEntry.do>

total exposure of 752.8 ks. This dataset does not include observations taken with imaging mode and those with the high energy transmission grating (HETG). A quick estimate indicates that these excluded observations would contribute additional $< 10\%$ to the total spectral counts, and thus our results will not be noticeably affected with or without them. For each employed observation, we used software package CIAO (version 4.3)⁴ and followed the standard procedure to re-calibrate, extract spectrum, and calculate the instrumental redistribution matrix file (RMF) and ancillary response file (ARF). For observations that used the Advanced CCD Imaging Spectrometer (ACIS) as the detector, we only utilized the first grating orders. The High Resolution Camera (HRC) does not have spectral resolution itself, and the spectral orders in observations with HRC cannot be sorted out. Therefore, for these observations, we calculated the RMFs and ARFs up to six grating orders and combined them as one in spectral analysis to account for contributions from different orders (see descriptions in Section 3). To improve spectral S/N, we utilized the user-developed IDL tools (Yao & Wang 2007) to combine the negative and positive spectral orders, coadd spectra of different observations, and calculate the averaged RMF and ARF by using the spectral counts around 20 Å as weights. The claimed two WHIM detections were based on a subset of the observations listed above (Nicastro et al. 2005; e.g., ObsIDs of 1715, 4148, and 4149⁵). To scrutinize the reported WHIM detections, we produced three coadded *Chandra* spectra and the corresponding RMFs and ARFs, based upon observations used by Nicastro et al. (Spectrum I), observations not included in their work (Spectrum II), and all observations together (Spectrum III), respectively. Figures 1-3 show six portions of these spectra.

The total 76 *XMM-Newton* observations were downloaded from the *XMM-Newton* science archive⁶. We used script package SAS (version 10.0)⁷ to reprocess these observations. To avoid the severe contamination from the background flares, for each observation we calculated the count rate on the chip CCD9, and created the good time intervals (GTIs) by excluding the time periods with rates higher than 0.2 counts per second. After this filter, there are 54 remaining observations, and each of them has the integrated GTIs longer than 5 ks. We then extracted spectra, calculated RMFs for each of exposures taken with the reflection grating spectrometer (RGS), and combined the spectra of these 54 observations and the corresponding RMFs by running the script *rgscombine* to get the final coadded spectrum (Spectrum IV; Figure 4), which has a total exposure of 1.2 Ms.

We used a binsize of 25 mÅ to re-bin all the coadded spectra, which is equivalent to an oversample factor of 2 for a ~ 50 mÅ resolution element of the LETG and RGS. Table 1 summarizes the S/Ns of these spectra.

3. SPECTRAL ANALYSES, RESULTS, AND DISCUSSION

Our goal in this section is to examine the WHIM detections at redshifts $z = 0.011$ and $z = 0.027$. Nicastro et al. (2005) reported the WHIM absorption from transitions of Ne ix K α , O vii K β , O viii K α , O vii K β , N vii K α , and C iv K α (Table 2 and Figure 8 in Nicastro et al. 2005), whose rest-frame

wavelengths are 13.447, 18.629, 18.969, 21.602, 28.787, and 33.736 Å, respectively (Verner et al. 1996). Therefore, we focus our attention on spectral ranges covering these transitions.

Obtaining a good continuum model is crucial to absorption-line measurement. Since all coadded *Chandra* spectra contain the contribution from HRC observations, to account for grating order-overlapping issues (Section 2), we decide to fit a broad range of the spectra from 7 to 40 Å, which covers the transitions to be examined. For a ease of comparison of three *Chandra* spectra, we jointly fit the Spectra I, II, and III. We first use a Galactic-absorption modified power-law (*wabs*powerlaw* in *xspec*) to fit the continuum emission, with neutral hydrogen column density N_H linked together while the power-law index Γ and normalization are allowed to vary. We obtain an unacceptable fit with $\chi^2 = 11646$ over 3590 degrees of freedom (DOF), and we find that some “broad” features cannot be accounted for by this simple model. These features are mainly due to imperfect instrumental calibration around node boundaries, CCD chip gaps plus dithering effects, the oxygen absorption edge, and imperfect cross calibration between ACIS and HRC observations (Marshall et al. 2004; Nicastro et al. 2005). We then use Gaussian profiles to compensate the uncounted calibration residuals. To minimize the effect of the known strong ISM absorption lines on continuum modeling, we include narrow absorption lines (with widths $\sigma \lesssim 50$ km s $^{-1}$) of O i, O ii, C vi, O vi, O vii, and Ne ix K α and O vii K β transitions at their rest-frame wavelengths (Verner et al. 1996; Juett et al. 2006; Yao et al. 2009) in our spectral fitting. The centroid energies and widths of these Gaussians are linked together while the normalizations are allowed to vary in the jointly spectral fitting. We find that, besides these narrow absorption lines produced in the ISM, we need 10 broad and one narrow Gaussian profiles to obtain an acceptable fit, and locations of these Gaussian are 10.53, 13.80, 14.60, 17.90, 18.19, 19.02, 19.10, 23.24, 23.31, 23.66, and 29.89 Å with widths (σ) of 0.61, 2.56, 0.04, 0.00054, 0.17, 1.36, 0.10, 1.45, 1.69, 0.41, and 0.39 Å. The final $\chi^2 = 4448.2$ with 3512 DOF and the constrained $N_H = 1.092 \pm 0.06 \times 10^{20}$ cm $^{-2}$, and $\Gamma = 2.131 \pm 0.001$, 2.011 ± 0.001 , 2.067 ± 0.001 for Spectra I, II, and III, respectively. *Because the absorption line measurement depends only on the local continuum, and because the centroids of these Gaussian profiles do not directly superpose on the wavelengths of the putative WHIM absorption lines, these Gaussian profiles will not have any effect on the line equivalent width measurement conducted below.* *XMM-Newton* spectrum (Spectrum IV) does not have the grating-order-overlapping issue, so we use the *wabs*powerlaw* model to fit the six narrow spectral ranges as plotted in Figure 4. We exclude the bad pixels in our spectral analysis, and obtain $\chi^2/DOF = 1.36, 1.49, 1.49, 1.28, 1.75, 1.56$ with DOF of 137, 75, 103, 105, 116 and 104, respectively. Figures 1-4 show these best fit continua with the ISM absorption lines removed from spectral models.

Now, let us examine the existence of the reported WHIM absorption lines. Figures 1-4 show the same portions of *Chandra* and *XMM-Newton* spectra as shown in Figure 8 of Nicastro et al. (2005), in which they demonstrated their detections of the WHIM absorption lines at $z = 0.011$ and $z = 0.027$ from transitions of Ne ix K α , O vii K β , O viii K α , O vii K β , N vii K α , and C iv K α . In particular, Figure 1 reproduces their Figure 8, as they were extracted from the same *Chandra* observations. Several bad pixels of the RGS accidentally

⁴ <http://cxc.harvard.edu/ciao/index.html>

⁵ Nicastro et al. (2005) in fact also included two additional HETG observations, which contributed negligible spectral counts to their final spectrum.

⁶ <http://xmm.esac.esa.int/xsa/index.shtml>.

⁷ <http://xmm.esac.esa.int/sas/>.

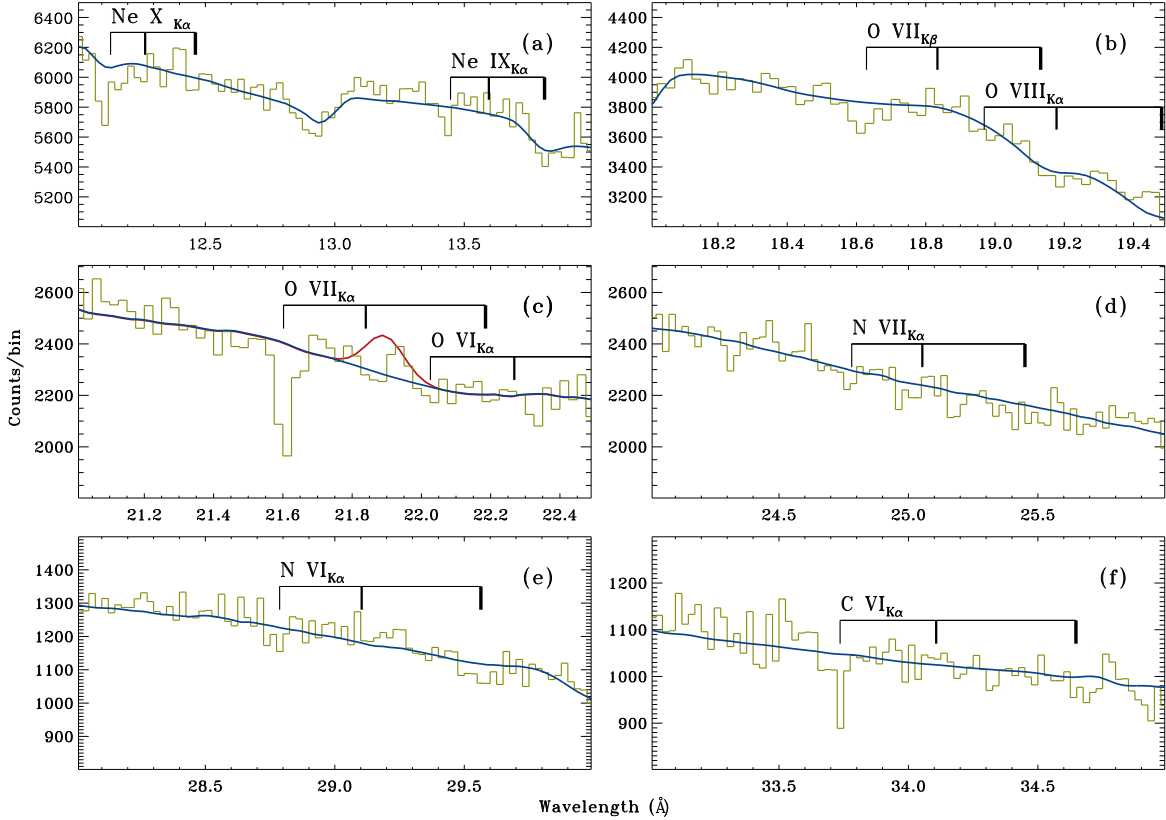


FIG. 1.— Six portions of coadded *Chandra*-LETG spectrum (green histogram) of Mrk 421 with the best-fit continuum model (blue curves). The model is convolved with the instrumental line spread functions. The binsize is 25 mÅ. The spectrum (Spectrum I) was extracted from the same observations as used by Nicastro et al. (2005), and the plots reproduce their Figure 8. $K\alpha$ and $K\beta$ transitions of eight ions covered by these spectral ranges are labeled in the plots, and the three vertical bars from left to right mark the corresponding rest-frame wavelengths (thin line), the expected wavelengths at $z = 0.011$ (medium line), and $z = 0.027$ (thick line). The red curve in panel (c) indicates the additional component added to local continuum in order to “amplify” the significance of the putative O VII $K\alpha$ absorption line at $z = 0.011$. The additional component is statistically unnecessary, and the red curve is for comparison purpose only. See text in Section 3 for details.

TABLE 1
SPECTRAL ANALYSIS RESULTS

line	redshift	S/N ¹	EW (mÅ) ¹	<i>Chandra</i>		S/N ³	EW (mÅ) ³	<i>XMM-Newton</i>	
				S/N ²	EW (mÅ) ²			S/N	EW (mÅ)
O VII ⁴	$z = 0$	68.9	10.9 ± 0.9	64.9	12.5 ± 0.9	94.5	11.7 ± 0.6	193.0	14.9 ± 0.6
	$z = 0.011$	67.6	< 3.0	62.8	< 1.5	92.2	< 1.6
	$z = 0.027^6$	66.2	< 3.1	60.6	< 1.5	89.6	< 2.0	187.4	< 1.6
O VII ⁵	$z = 0$	68.9	11.3 ± 1.0	64.9	11.8 ± 1.1	94.5	11.6 ± 0.9
	$z = 0.011$	67.6	3.3 ± 1.2	62.8	< 2.0	92.2	2.0 ± 1.1
	$z = 0.027^6$	66.2	< 3.3	60.6	< 1.5	89.6	< 2.0

NOTE. — The S/N is given per 50 mÅ resolution element around the lines, and EW is the measured equivalent width. Error ranges are quoted at 1σ significance level, while the upper limits are at 3σ .

¹ Measurements are obtained from the spectrum corresponding to observations used by Nicastro et al. (2005) (Spectrum I; Figure 1).

² Measurements are obtained from the spectrum corresponding to those observations not used by Nicastro et al. (Spectrum II; Figure 2).

³ Measurements are obtained from the spectrum corresponding to all observations (Spectrum III; Figure 3).

⁴ EW measurements in these three rows are obtained from the best-fit continua without compensation of the 11th broad Gaussian (blue curves in Figures 1-4).

⁵ EW measurements in these three rows are obtained from the best-fit continua with compensation of the 11th broad Gaussian (red curves in Figures 1-3). However, since the 11th broad Gaussian profile is statistically unnecessary, these measurements are for comparison purpose only.

⁶ The measured upper limits to EW of the O VII $K\alpha$ are obtained by fixing the line centroid at $z = 0.028$ instead of $z = 0.027$, since Nicastro et al. (2005) reported O VII line at the former redshift.

See text for details.

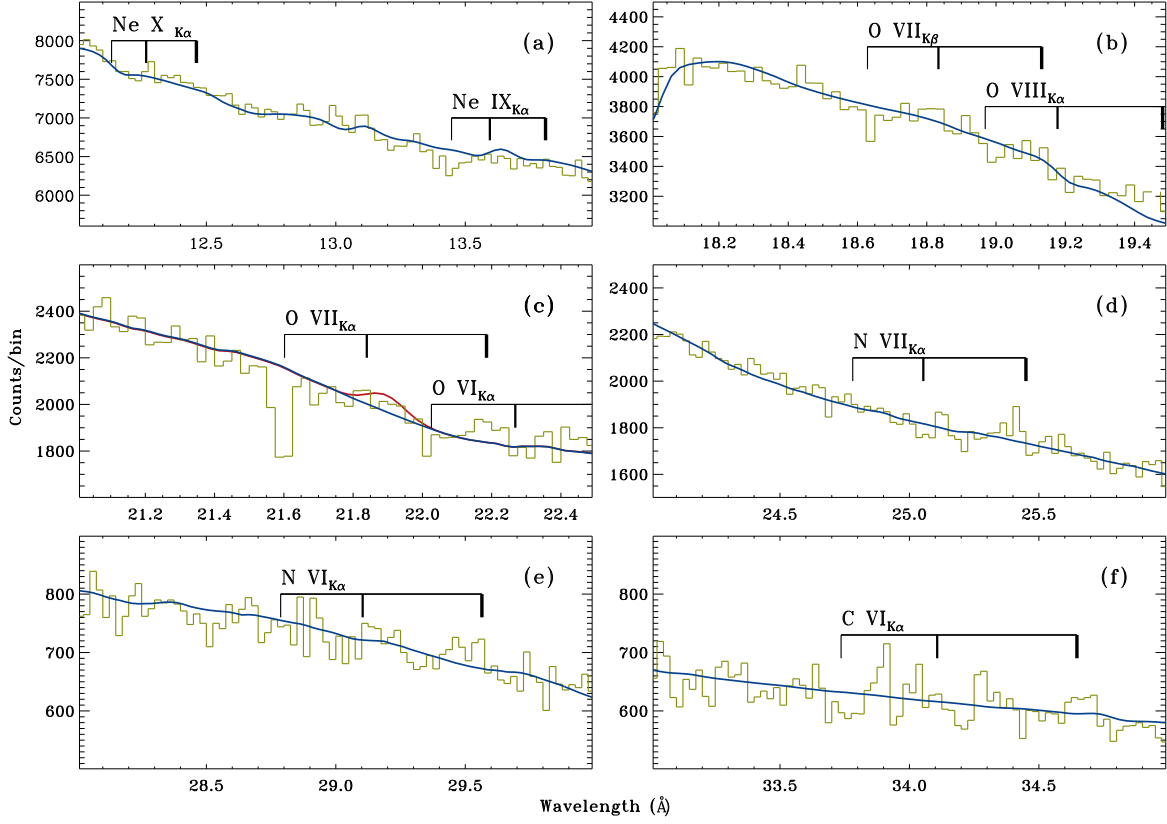


FIG. 2.— Same as Figure 1, except that the spectrum (Spectrum II) was extracted from the newly available *Chandra*-LETG observations.

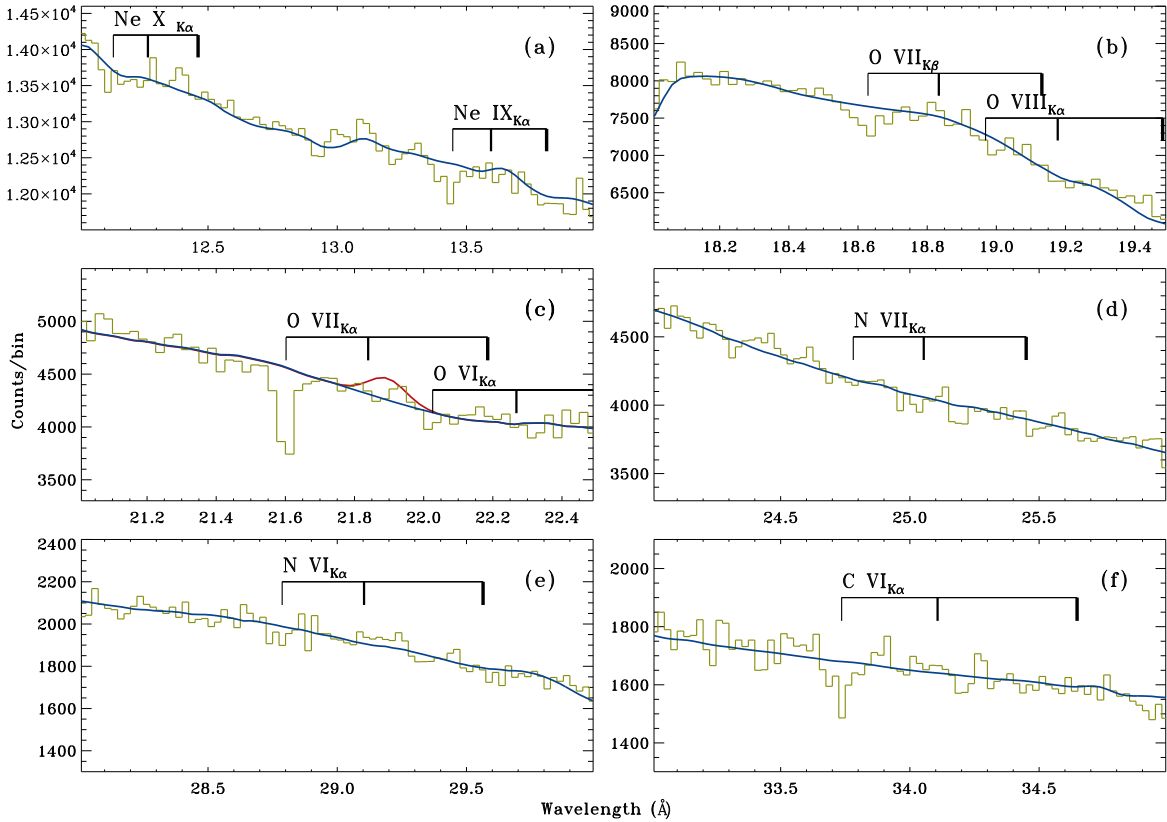


FIG. 3.— Same as Figure 1, except that the spectrum (Spectrum III) was extracted from all available *Chandra*-LETG observations.

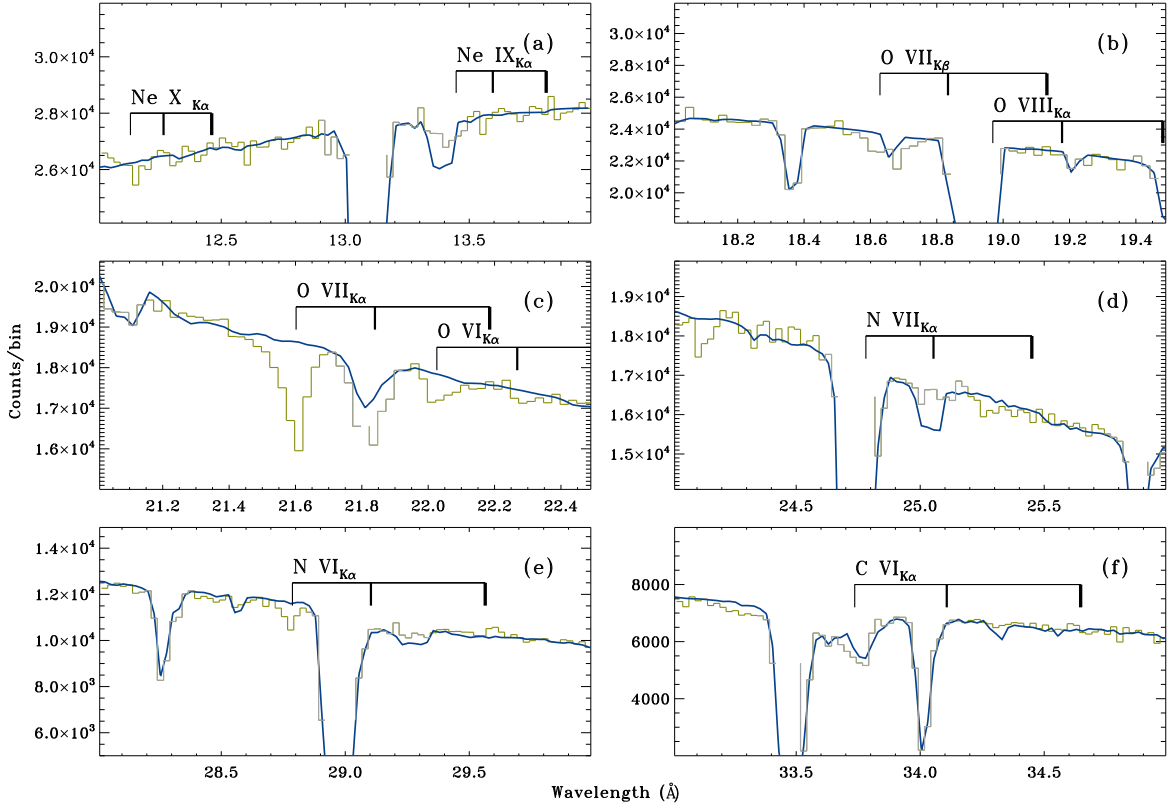


FIG. 4.— Same as Figure 1, except that the spectrum (Spectrum IV) was extracted from all available *XMM-Newton*-RGS observations. Channels/bins colored as grey were contaminated by hot pixels and were ignored in our spectral analysis. Panels (b)-(f) were extracted from the RGS1 observations, and panel (a) was extracted from the RGS2 observations.

fall around the 21.8 Å region and cause an instrument feature (Figure 4). Although a careful calibration could yield a correct instrumental response of the RGS, in this work we do not use the *XMM-Newton* spectrum to assess the WHIM detection at $z = 0.011$. Visual inspection reveals that none of the above WHIM lines reported by Nicastro et al. (2005) is detected in the previously *Chandra* observations they analyzed (Figure 1), and in the newly available *Chandra* observations (Figure 2), and in the *XMM-Newton* observations (Figure 4).

The reported WHIM detections could be due to the improper continuum placement on the spectrum. Visual inspection also reveals that there might be an absorption feature at ~ 21.8 Å in Spectrum I, which corresponds to the reported O VII K α WHIM absorption line at $z = 0.011$ (panel (c) in Figure 1). However, such an absorption feature is not visible in Spectra II and III (panel (c) in Figures 2 and 3), and its significance in Spectrum I depends largely on how the local continuum is placed. Please note that our spectral profiles of the local continua were obtained by jointly fitting the Spectra I, II, and III (see above), and the best-fit model seems to account for the general spectral variation reasonably well. To quantitatively assess the existence of the O VII K α WHIM line at $z = 0.011$, in the joint analysis of the Spectra I, II, and III, in addition to the 10 Gaussian profiles, we add the 11th “broad” Gaussian to the local continuum and another narrower Gaussian with width ⁸ $\sigma = 50$ km s⁻¹ to represent the WHIM absorption line. Again, we link the line centroids and widths together in our joint fitting but allow the normalizations to

vary among the Spectra I, II, and III. The best fit yields a line centroid of 21.90 Å and $\sigma = 0.050$ Å for the “broad” component and a centroid of 21.87 Å for the narrow component. The red curves in panel (c) of Figures 1-3 show the modified local continua. These additional components reduce the χ^2 of 26.4 by adding nine DOF in total. However, applying the best-fit models to individual spectra yields a χ^2 change of 13.7, 4.3, and 10.4 by introducing five additional DOF to spectral fitting of Spectrum I, II, and III, respectively. All these *Chandra* spectra can be well described by the same continuum profile with various normalizations, which has been proved to be reasonable to other wavelength ranges (panels (a)-(b) and (d)-(f) in Figures 1-3). Because we find essentially no improvement in fitting the Spectrum II, adding the “broad” Gaussian profile to the local continuum around 21.9 Å is statistically unnecessary.

We next attempt to measure the equivalent widths (EW) of the putative WHIM absorption lines. Since we have not consistently detected any WHIM absorption of any transitions reported by Nicastro et al. (2005), we focus here on measuring the upper limit to the equivalent width (EW) of the O VII K α line, which is expected to be the most abundant transition in a broad temperature range of the WHIM (Section 1). At redshifts $z = 0.011$ and $z = 0.027$, the rest-frame O VII K α at 21.60 Å is shifted to 21.84 and 22.19 Å, respectively, and therefore our measurements are obtained from the spectral range described by the continuum colored as blue in panel (c) of Figures 1-4. To make a fair comparison with the results obtained by Nicastro et al. (2005), we also make similar measurements by using the continuum colored as red. We should emphasize that the latter measurements are only for comparison pur-

⁸ Different widths yield nearly identical results as long as the line is still unresolved by the instrument. Please see Section 4.1 for justifications for the line width.

poses, since the additional component to the local continuum that “amplifies” the significance of the absorption line at 21.8 Å is statistically unnecessary. Our results are reported in Table 1.

In summary, our analysis and results do not support the existence of the two WHIM systems at $z = 0.011$ and $z = 0.027$. We analyze all the available *Chandra* and *XMM-Newton* observations of Mrk 421, and have not seen any consistent WHIM absorption of any transition at either $z = 0.011$ or $z = 0.027$ reported by Nicastro et al. (2005). We measure the EW of the O VII K α absorption line. For the system at $z = 0.027$, we obtain a firm 3σ upper limit of $EW < 1.5$ mÅ from the spectrum (Spectrum II) extracted from the newly available *Chandra* observations, in contrast to $EW = 2.2 \pm 0.8$ mÅ obtained by Nicastro et al. For the system at $z = 0.011$, we confirm the existence of a small dip in the spectrum (Spectrum I) identical to that used by Nicastro et al. (2005), but the similar spectral feature is absent in Spectrum II. The measurement of the line heavily depends on how the local continuum is placed, and the additional spectral component that amplifies its significance is statistically unnecessary. We obtain an upper limit of $EW < 1.5$ mÅ from the new spectrum, in contrast to $EW = 3.0^{+0.9}_{-0.8}$ mÅ reported by Nicastro et al. (2005). The findings in this work are consistent with the previous investigation made by Kaastra et al. (2006), in which the authors scrutinized the same data set used by Nicastro et al. and a subset of calibration observations of *Chandra* and *XMM-Newton*. Therefore, we conclude that there is no WHIM line detected at either $z = 0.011$ or $z = 0.027$ along the Mrk 421 sight line.

There are also other important absorption lines in the spectral range of interest (Figures 1-4). The prominent lines are O VII, Ne IX, and C IV K α and O VII K β at $z \approx 0$, and the O VI K α with rest-frame wavelength 22.0 Å at $z \approx 0$ is also visible in all four spectra albeit less significant. Again, we only measure the EWs of O VII K α and report them in Table 1. The O VII line at $z \approx 0$ can be well explained as absorption from the Galactic diffuse interstellar medium (ISM) (Yao & Wang 2007), and the O VI line is also believed to originate from the ISM (Savage et al. 2005). It is worth noting that the EW of O VII K α at $z \approx 0$ measured from *XMM-Newton* observations is $\gtrsim 3\sigma$ larger⁹ than that obtained from *Chandra* observations (Table 1). Such a discrepancy in O VII has also been measured by Kaastra et al. (2006). The causes to this discrepancy are still under investigation, and the results will be published elsewhere. In this paper, we mainly focus on X-ray absorption measurements of the WHIM and will not discuss these non-WHIM measurements any further.

4. BOOTSTRAP SIMULATIONS

In Sections 2 and 3, we reprocessed all the available observations and obtained two spectra with the highest S/Ns ever collected with *Chandra* and *XMM-Newton*. Despite the increased S/N, we still cannot confirm the X-ray WHIM detections reported by Nicastro et al. (2005). Given such a frustrating situation (see also discussions in Section 1), several crucial questions need to be answered before further major time allocations search for the WHIM through X-ray absorption line measurement: How high S/Ns are needed to firmly

establish a WHIM detection? What is the O VII column density range suitable for *Chandra* and *XMM-Newton* to explore with reasonably long exposure time? Is it possible to conduct a systematic study of the WHIM using the current X-ray telescopes? If not, what are the requirements for next-generation X-ray telescopes?

4.1. Expected WHIM properties and required instrumental sensitivities

Before running bootstrap simulations to address these questions, we first review the WHIM properties based on the results of numerical simulations. We then estimate the required instrumental sensitivity to detect the WHIM by answering the following two specific questions: First, what O VII column density is needed to probe the majority of the baryons contained in the O VII-bearing WHIM? Cosmological simulations predict different O VII column density distributions per unit redshift with different recipes for galactic feedback and intergalactic photoionization (Fang et al. 2002b; Cen & Fang 2006; Smith et al. 2012). In Figure 5 we convert two recent distributions (Figure 5 in Cen & Fang 2006 and figures in Smith et al. 2012) to the fraction of baryons contained in the O VII-bearing WHIM as a function of O VII column density. In this conversion, we assume a single temperature and uniformly distributed metallicity for all absorbers. However, Smith et al. (2012) find covariance between N_{OVII} and metallicity, and the WHIM is expected to be multiphase. To obtain a more realistic distribution, one should consider the ionization and metallicity correction together. However, without a detailed description of the WHIM properties (which in fact are our final goals), such a correction is difficult to apply. Considering the general trend that higher column density absorbers have higher metallicity, the plotted baryon fractions contained in the higher column absorbers (e.g., $N_{\text{OVII}} \gtrsim 10^{15} \text{ cm}^{-2}$) should be regarded as upper limits. Furthermore, since there is no clear sign of convergence at low column densities (Cen & Fang 2006; Smith et al. 2012), in our conversion we use a 4- or 6-degree polynomial to fit the number density distributions, which artificially generate turnover at column densities $10^{10} - 10^{12} \text{ cm}^{-2}$. The low column density absorbers could contain even more baryons if the distributions converge at lower columns. Nevertheless, Figure 5 gives an estimate of the baryon fraction distribution, which indicates that $\sim 55\%$ (or 65% or 80%, depending on which simulation is selected) of baryons are contained in absorbers with $N_{\text{OVII}} > 10^{14.5} \text{ cm}^{-2}$ and that $\sim 30\%$ (or 45% or 55%) of baryons are contained in absorbers with $N_{\text{OVII}} > 10^{15} \text{ cm}^{-2}$.

Another important, yet to be determined property is the dispersion/Doppler velocity b_v of the O VII-bearing gas. This property, although not essential for the detectability of *Chandra* and *XMM-Newton* (Section 4.2), is important for estimating the required spectral resolution of future X-ray instruments (Section 4.3). Here we use O VI as a reference. Assuming most detected IGM O VI tracing the WHIM at temperatures $\sim 10^{5.5} \text{ K}$ and the total b_v being a combination of thermal and turbulent motions through quadrature $b_v^2 = b_{\text{th}}^2 + b_{\text{turb}}^2$, the median $b_v \sim 30 \text{ km s}^{-1}$ of the O VI absorption lines (Danforth & Shull 2008; Tripp et al. 2008) suggests a turbulent velocity of $b_{\text{turb}} \sim 24 \text{ km s}^{-1}$ for the O VI-bearing gas. Higher temperature gas may have higher turbulent velocity. Thus b_v of the O VII-bearing gas at temperatures $\sim 10^6 \text{ K}$ is expected to be $> 40 \text{ km s}^{-1}$. Another useful reference is the

⁹ The differential significance is calculated as

$$|EW_1 - EW_2| / \sqrt{(\Delta EW_1)^2 + (\Delta EW_2)^2},$$

where ΔEW is the 1σ error of EW measurement.

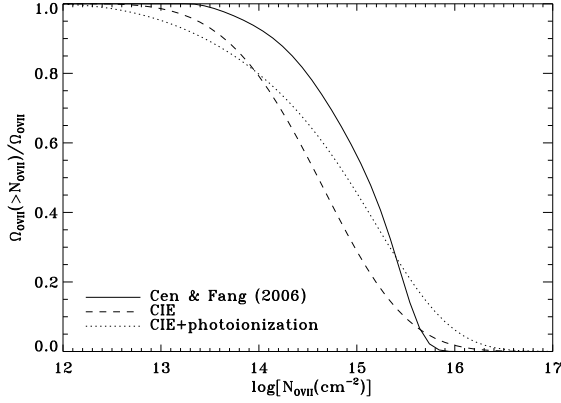


FIG. 5.— Fraction of baryons contained in the O VII-bearing gas as a function of O VII column density. The solid line is derived from Figure 5 in Cen & Fang (2006). The dashed and dotted lines are derived from figures in Smith et al. (2012), which consider collisional ionization (CIE) only and CIE plus photoionization, respectively. See text for details.

hot phase Galactic ISM traced by the O VII absorption line at $z \approx 0$, although the IGM environment could be substantially different from the ISM. Nevertheless, along the Mrk 421 and LMC X-3 sight lines, the b_v of the O VII gas can be as large as 100 km s^{-1} (Wang et al. 2005; Yao & Wang 2007; Yao et al. 2009). We therefore will explore three b_v values, 50, 75, and 100 km s^{-1} , in our simulations.

Second, what is the flux limit that X-ray telescopes should reach in order to statistically investigate the WHIM? The answer to this question depends largely on how many WHIM systems are planned to detect. Clearly when more systems are detected, one can investigate WHIM properties, like thermal and dynamic properties, metallicities, and their evolution with redshift. To obtain a spectrum with a requested S/N, the required exposure time is inversely proportional to the flux of a QSO. And the higher the redshift of a QSO, the higher possibility there is intervening WHIM absorbers along the line of sight. Therefore, to estimate the number of WHIM systems that could be detected, one should create a target list by considering the QSO redshift and flux as a whole.

In this work, instead of providing a target list for the WHIM investigation, we require that future X-ray telescopes be able to observe and search for the corresponding O VII absorbers along the majority of the sight lines where IGM O VI absorbers have already been reported (Section 1). In this regard, we examine the target lists in Danforth & Shull (2008) and Tripp et al. (2008) and find that there are ~ 80 IGM O VI systems along 28 QSO sight lines reported so far. Among them, we have assembled the available soft X-ray fluxes¹⁰ for 24 sight lines from the bright source catalogs of *Einstein*, *ASCA*, *BeppoSAX*, and *ROSAT*, and from several pointing observations with *XMM-Newton* and *Chandra* (Wilkes & Elvis 1987; Ueda et al. 2005; Reeves & Turner 2000; Verrecchia et al. 2007; Bianchi et al. 2009; Papadakis et al. 2007; Foschini et al. 2006; Porquet et al. 2004; White et al. 2000; Leighly et al. 2007). These fluxes range from 0.006 to 46.5 mCrab with a median of ~ 0.3 mCrab. Fifteen of them have fluxes $\gtrsim 0.2$ mCrab and sample a total redshift pathlength of $\Delta z = 2.1$. For the WHIM O VII-absorbers with $N_{\text{O VII}} > 10^{15} \text{ cm}^{-2}$, Cen & Ostriker (2006) predicted the absorber frequency to be $dN/dz \sim 7$, and Smith et al. (2012) predicted the fre-

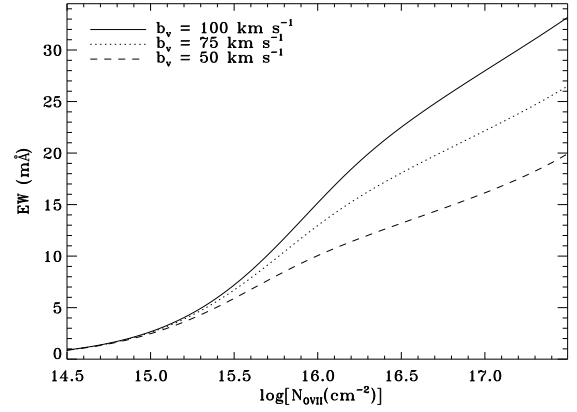


FIG. 6.— Curve of growth of the equivalent width of O VII K α absorption line versus O VII column density with three different Doppler dispersion velocities (b_v).

quency to be ~ 20 considering collisional ionization only and $dN/dz \sim 5$ if photoionization is included. For absorbers with $N_{\text{O VII}} > 10^{14.5} \text{ cm}^{-2}$, dN/dz is predicted to be ~ 18 , 12, and 110, respectively. Therefore, X-ray telescopes should be able to facilitate absorption line study from background sources with flux of ~ 0.2 mCrab, and ≥ 10 WHIM systems with $N_{\text{O VII}} > 10^{15} \text{ cm}^{-2}$ and ≥ 24 systems with $N_{\text{O VII}} > 10^{14.5} \text{ cm}^{-2}$ are expected in these sources along which the corresponding O VI absorptions are already known.

4.2. Detection limits of current X-ray telescopes

We now use bootstrap simulations to examine the detectability of *Chandra*-LETG and *XMM-Newton*-RGS. In our simulations, we utilize the user-developed absorption line model *absline* (Yao & Wang 2005) to model O VII absorbers with column density $N_{\text{O VII}}$ and dispersion velocity b_v , and use a PL continuum to model an emission spectrum. With the input parameters of $N_{\text{O VII}}$, b_v , PL normalization, and an exposure time, we simulate two spectra within Xspec, using the RMFs and ARFs produced in Section 2, to mimic *Chandra* observations and *XMM-Newton* observations, respectively. From the simulated spectra, we use a Gaussian profile to represent the absorption line and measure its EW and uncertainty ΔEW at the expected wavelength position and then calculate the line SL (Eq. 2). For a set of parameters, we repeat this procedure 1000 times and record the measurement SL of the line. We then sort the SL and select the 100th value (i.e., 90% simulation trials yield the SL equal to or higher than the selected value). We make the same measurement for various combinations of different exposure times, b_v , and $N_{\text{O VII}}$. Since the full-width-half-maximum (FWHM) of the LSF of both *Chandra*-LETG and *XMM-Newton*-RGS is $\sim 50 \text{ mÅ}$, which is much broader than the expected b_v values of the WHIM O VII absorbers (Section 4.1), all simulated absorption lines appear unresolved. What really matters for measurement is the effective EW of an absorption line. To provide a direct comparison to observations, we convert the combination of $N_{\text{O VII}}$ and b_v to EW through the curve-of-growth (COG), and the combination of exposure time, RMF, and ARF to S/N per 50-mÅ resolution element. For reference, we plot the COG of O VII K α line in Figure 6.

Figure 7 shows our simulation results. Taking the simulations for *Chandra*-LETG for an example, our results can be interpreted as: from a spectrum with S/N = 50 per resolution element, an O VII K α absorption line with EW = 3.4, 5.7, 8.1, 10.3 mÅ can be measured at $\gtrsim 2, 4, 6$ and 8σ SLs, respec-

¹⁰ We use a power-law form $f(E) \sim E^{-1.1} dE$ to convert the reported flux to the energy range of 0.5-2.0 keV (Section 1).

tively, in 900 out of 1000 observations. In another word, to measure the absorption line with these EWs at 2, 4, 6 and 8 σ or higher SLs, a spectrum with $S/N \geq 50$ is required. Interestingly, the measured line significances behave nicely like PL functions in the EW-S/N space. For reference, we formulize them as,

$$\log(EW) = \alpha \times \log(S/N) + \sum_{i=0}^3 \beta_i \times SL^i, \quad (2)$$

where SL is 2, 3, 4, 5, 6, 7, or 8. For *Chandra* simulations, $\alpha = -0.932$, $\beta_{0-3} = 1.79108, 0.188439, -0.0148031$, and 0.000476159 , and for *XMM-Newton*, $\alpha = -0.970$, $\beta_{0-3} = 2.14183, 0.217703, -0.0197475$, and 0.000748764 .

Let us use our simulation results to further examine the two putative WHIM systems. In Figure 7, we also plot the EWs reported by Nicastro et al. (2005) and their 1σ errors at the corresponding S/N positions of Spectrum I. We find that their reported SLs appear to be consistent with expectations of our simulations. However, we stress again that their SL measurement could have been largely impacted by the improper continuum placement (Section 3). Our simulations indicate that an O VII K α absorption line with $EW=3.0$ mÅ at $z = 0.011$ (Nicastro et al. 2005) should be measured at $\geq 3.7\sigma$ SL from *Chandra* Spectrum III with $S/N \sim 92$ (Eq. 2; Figure 7). This is in contrast to the fact that we only obtain an upper limit (Figure 3; Table 1). At $z = 0.027$, an O VII line with $EW = 2.2$ mÅ should be detected at $\gtrsim 2.3\sigma$ from the coadded *Chandra* and *XMM-Newton* spectra, which, again, is in contrast to the fact that we only obtain upper limits. We therefore conclude that the putative O VII WHIM absorptions, if they exist at all, must have lower EWs than reported.

Is the reported WHIM absorption at $z = 0.027$ associated with a galaxy filament? Williams et al. (2010) discovered a filament of late-type galaxies at $z = 0.027$, suggesting a possible association between the reported WHIM absorber and the filament. In the spectrum of PKS 0405-123 observed with the Cosmic Origins Spectrograph (COS) aboard the *Hubble Space Telescope*, a similar association has also been suggested by a broad O VI absorption line (Savage et al. 2010). The authors estimated that the WHIM contained within the abundant late-type galaxy groups could make up to 15% of the total baryons in the local universe. However, the non-detection of O VII at $z = 0.027$ in this work leads us to conclude that there is, if at all, much less O VII than reported. A recent search in a high-S/N COS spectrum of Mrk 421 also failed to find any absorption feature of BLA at the redshift (Danforth et al. 2011). Similarly, there is no detected hot intragroup O VII-bearing gas in our Local Group (Fang et al. 2006; Yao & Wang 2007; Bregman 2007). Therefore, if there is any gas associated with the galaxy filament at $z = 0.027$ along the Mrk 421 sight line, it must be at higher temperatures ($T > 10^{6.5}$ K) and/or be metal poor and thus contain too little O VII and H I to be detected.

Our simulation results also have important implications for using current X-ray observatories to search for the WHIM absorption. First, *Chandra* and *XMM-Newton* can probe the WHIM absorbers with $N_{OVII} \gtrsim 10^{16} \text{ cm}^{-2}$ with exposure times of ~ 1 Ms from a QSO spectrum with a flux of ~ 0.2 mCrab. The O VII column densities correspond to EWs of $\gtrsim 10-15$ mÅ (Figure 6), which require a *Chandra* (*XMM-Newton*) spectrum with $S/N = 18-27$ ($41-63$) to measure it at $\gtrsim 4\sigma$ significance levels (Figure 7; Eq. 2). To col-

lect a spectrum with such S/N, takes 1.4–3.1 Ms for *Chandra* (adopting $A = 20 \text{ cm}^2$ effective area) and 3.6–8.5 Ms for *XMM-Newton* (adopting $A = 40 \text{ cm}^2$ effective area) from a QSO with 0.2 mCrab flux. This is consistent with the commonly detected O VII absorption lines, which trace the Galactic hot ISM, in the spectra of local QSOs ($z \lesssim 0.1$) with fluxes > 2 mCrab (Fang et al. 2006; Bregman 2007; Yao & Wang 2007). However, the simulated dN/dz of O VII drops by about two orders of magnitude between $N_{OVII} > 10^{15} \text{ cm}^{-2}$ and $N_{OVII} > 10^{16} \text{ cm}^{-2}$ (Smith et al. 2012), meaning that such high column O VII-absorbers are extremely rare and may only exist in the circumgalactic environment around galaxy structures (e.g., Fang et al. 2010).

Second, it is likely infeasible to conduct a systematic study of the WHIM with *Chandra* or *XMM-Newton*. The EW for $N_{OVII} = 10^{15} \text{ cm}^{-2}$ is ~ 2.5 mÅ (Figure 6), which requires a spectrum with $S/N \sim 120$ (*Chandra*) and 260 (*XMM-Newton*) to measure it at $\sim 4\sigma$ significance level (Figure 7). It would require 61 Ms for *Chandra* and 144 Ms for *XMM-Newton* to collect a spectrum with such a high S/N from a QSO with 0.2 mCrab flux. Even for a blazar at its burst state like Mrk 421, it still takes 0.6 (1.4) Ms *Chandra* (*XMM-Newton*) time from the source continuously being bright at 50 mCrab level. It would take 341 Ms for *Chandra* and 804 Ms for *XMM-Newton* to complete the survey of the 15 background QSOs with fluxes $\gtrsim 0.2$ mCrab along which IGM O VI has been reported (Section 4.1). Furthermore, since the expected WHIM O VII absorption lines cannot be resolved, it is impossible to study the dynamics of the WHIM with either *Chandra*-LETG or *XMM-Newton*-RGS. Clearly, we need new X-ray spectrographs with much improved spectral resolution and much larger collecting area to systematically study the WHIM.

4.3. Requirement for next generation X-ray telescopes

The goal in this section is to establish the required spectral resolution and effective area for next generation X-ray telescopes. Since there is no existing X-ray telescope with spectral resolution better than those of *Chandra* and *XMM-Newton*, we use Gaussian profiles to simulate the LSFs of the putative X-ray spectrographs. We assume a spectral resolution, which is defined¹¹ as $R = \lambda/\Delta\lambda$, of 1500, 3000, 4000, and 6000, respectively, with effective area of $A = 1000 \text{ cm}^2$ throughout the whole wavelength coverage. We use four spectral bins within a FWHM spectral range (i.e., an oversample factor of 4) in our simulations. With a set of selected R , N_{OVII} , and b_v of the O VII-bearing gas, we follow the same procedure as described in Section 4.2 to simulate an absorption spectrum of an background source with 0.2 mCrab flux for an assumed exposure time, and then measure the EW and ΔEW from the simulated spectrum. We repeat the procedure 1000 times and select the SL value so that 90% trials have the same or higher SL. In a real observation, background source flux, instrumental effective area, and exposure time can compensate each other, so we define their product (FAE) as a figure of merit. Figure 8 shows our simulation results. For reference, we also label the corresponding EW to the labeled N_{OVII} at top X-axis of the plots. Table 2 summarizes the required exposure time for the future spectrograph with 1000 cm^2 effective area and different spectral resolutions to constrain the O VII absorption with $N_{OVII} = 10^{15} \text{ cm}^{-2}$ and three different b_v values at > 4 and 6σ significance levels from a background source

¹¹ We use the FWHM of the LSF as $\Delta\lambda$.

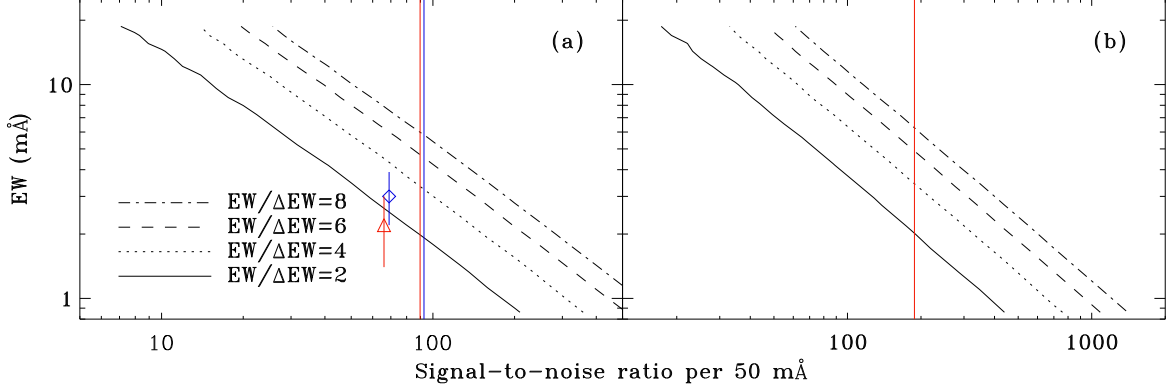


FIG. 7.— The 2, 4, 6, and 8σ detection significance of O VII $K\alpha$ versus S/N per 50-mÅ resolution element with *Chandra*-LETG (a) and *XMM-Newton*-RGS (b). The vertical red and blue lines mark the S/N levels of the final coadded spectra around the clamed O VII lines at $z = 0.027$ and $z = 0.011$, respectively. The red triangle and blue diamond indicate the detections and their 1σ ranges reported by Nicastro et al. (2005). In simulations, the instrumental response files were taken from *Chandra* observation with ID 4148 and *XMM-Newton* observation with ID 0099280201.

TABLE 2

R	Dispersion velocity b_v		
	50 km s ⁻¹	75 km s ⁻¹	100 km s ⁻¹
1500	416.9 (808.8)	398.8 (794.6)	414.6 (799.5)
3000	217.4 (433.9)	237.6 (492.6)	277.8 (549.9)
4000	171.1 (350.3)	212.1 (425.7)	241.2 (523.0)
6000	126.3 (276.5)	162.9 (368.2)	208.3 (461.7)

NOTE. — Required exposure times in unit of ks for future X-ray spectrographs with various spectral resolutions to obtain $> 4\sigma$ significance measurement of O VII $K\alpha$ with $N_{\text{OVII}} = 10^{15} \text{ cm}^{-2}$ and different dispersion velocities. The values in parentheses are required exposures for $> 6\sigma$ constraint (Figure 8).

with 0.2 mCrab flux.

Our simulations results deserve some explanation. First, each significance contour has a steep PL plus a relatively flat floor in the logarithm FAE- N_{OVII} space, which roughly corresponds to the shape of the COG (Figure 6). The transition locations indicate the column densities from which the saturation of a line begins to affect the measurement. Second, to constrain $N_{\text{OVII}} = 10^{15} \text{ cm}^{-2}$ at the same significance levels, it takes an increasingly long time with increasing b_v for all resolutions except for $R = 1500$ (Table 2). This is mainly due to line broadening. With $R = 1500$, no lines with $b_v < 120 \text{ km s}^{-1}$ can be resolved, since the intrinsic line width is narrower than the instrumental LSF. Therefore the simulations are analogous to those for *Chandra* and *XMM-Newton*, which explains the required exposure times being essentially same for all b_v values. At $R \gtrsim 3600$, a line with $b_v > 50 \text{ km s}^{-1}$ becomes resolved. Because the column density $N_{\text{OVII}} = 10^{15} \text{ cm}^{-2}$ lies on the linear part of the COG (Figure 6), an increased b_v does not increase the EW but broadens the line profile, and therefore requires longer exposure to pick up the absorption signals from the continuum.

A spectrograph with spectral resolution of $R \gtrsim 3600$ is required to resolve the expected WHIM O VII absorption lines. As we discussed in Section 4.1, the lower limit to the dispersion velocity of the WHIM O VII absorbers is expected to be $b_v \gtrsim 50 \text{ km s}^{-1}$, which is equivalent to a FWHM of 83.3 km s^{-1} for a Gaussian profile fit. Although we can measure b_v by comparing the different saturation levels of the $K\alpha$ and $K\beta$ transitions of O VII from the “low” resolution observations made with *Chandra* and *XMM-Newton* (e.g., Yao & Wang 2005, 2007), such technique cannot be applied to a column density as low as $N_{\text{OVII}} \sim 10^{15} \text{ cm}^{-2}$ because saturation is neg-

ligible and the $K\beta$ line becomes too weak to be detectable. Therefore, we have to rely on the instrumental resolution ($R \sim 3600$) to resolve the line and obtain the dynamical and kinematic information of O VII-absorbers. Please note that, to date, the X-ray spectrograph with the highest spectral resolution is the High Energy Transmission Grating Spectrograph (HETGS; Canizares et al. 1986) aboard on *Chandra*, which has two sets of gratings: the high energy grating (HEG) and medium energy grating (MEG) with resolutions of ~ 1700 and 900 at 20 \AA . Clearly, they are still not high enough for resolving the expected WHIM absorption line. Furthermore, the small effective area ($< 1 \text{ cm}^2$ and $\sim 2 \text{ cm}^2$) around 20 \AA makes the HETGS infeasible for the task discussed here (please also see below). Figure 9 shows the necessity for high spectral resolution by comparing the LSFs of *XMM-Newton*, *Chandra*, and a next-generation X-ray spectrograph with $R = 4000$ and the corresponding simulated spectra. It demonstrates that an absorber with two velocity components separated by 150 km s^{-1} cannot be resolved by *XMM-Newton* (*Chandra*) even from a spectrum with S/N as high as 350 (200), but it can be clearly resolved by the next-generation spectrograph from a spectrum with S/N ~ 30 .

With $R = 4000$, an effective area of $A \geq 100 \text{ cm}^2$ is needed for the spectrograph to systematically survey the WHIM O VII along 15 sight lines within 6 months. Assuming that all O VII absorbers have $b_v = 75 \text{ km s}^{-1}$, it would take 11.2 Ms for a spectrograph with $R = 4000$ and $A = 100 \text{ cm}^2$ to finish surveying those 15 QSOs with $\gtrsim 0.2 \text{ mCrab}$ (Section 4.1) and measure the intervening WHIM absorbers with $N_{\text{OVII}} \sim 10^{15} \text{ cm}^{-2}$ at $\geq 4\sigma$ significance. Assuming a 70% on-target timing efficiency, this is equivalent to a half year. To constrain the absorbers with $N_{\text{OVII}} \sim 10^{14.5} \text{ cm}^{-2}$ with the same amount of exposure time, $A = 1000 \text{ cm}^2$ is required (Figure 8).

In this section, we focused on the instrumental requirement particular for the study of the WHIM. In fact, X-ray absorption/emission line diagnostics can also provide essential information for the physics of the ISM, stellar coronae, black hole accretion and outflow, quasar accretion and feedback, etc., and remarkable progress has already been made with *Chandra* and *XMM-Newton* observations (e.g., Yao & Wang 2006; Testa et al. 2008; Miller et al. 2006; Arav et al. 2007). With an X-ray spectrograph equipped with $R \sim 4000$ and $A \sim 100 \text{ cm}^2$, we should be able to explore all these fields in great detail.

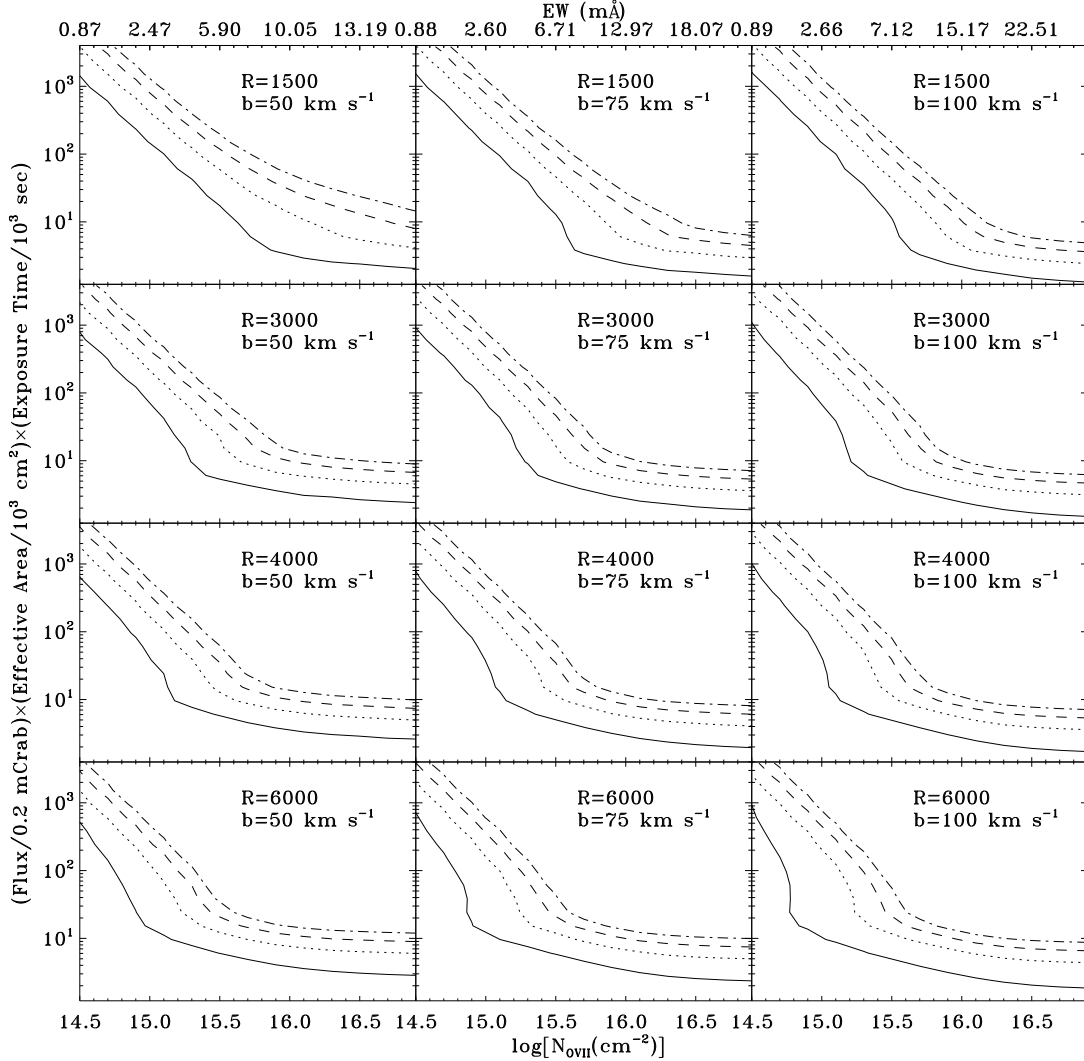


FIG. 8.— The required exposures for detecting O VII K α line at 2, 4, 6 and 8 σ significance levels (corresponding to curves from bottom to top in each panel) for the absorbing gas with dispersion velocities of 50, 75, and 100 km s $^{-1}$ (panels from left to right) and column densities $\log N_{\text{O VII}}(\text{cm}^{-2}) = 14.5 - 17.0$. The top X-axis shows the corresponding equivalent width in mÅ. The simulations used flux integrated from 0.5–2 keV and assumed a Gaussian profile of the line spread function of a spectrograph with spectral resolution $R \equiv \lambda/\text{FWHM} = 1500, 3000, 4000, 6000$ (panels from top to bottom), respectively.

5. SUMMARY

1. We analyzed all available (as of 2011 April) grating data and obtained two coadded spectra with S/N \sim 90 per 50-mÅ resolution element from *Chandra* observations, and S/N \sim 190 from *XMM-Newton* observations. Neither *Chandra* nor *XMM-Newton* observations support the existence of the two WHIM systems previously reported by Nicastro et al. (2005).

2. We ran bootstrap simulations for the detecting limits of the current X-ray telescopes. We find that the reported EWs of the O VII K α at $z = 0.011$ and $z = 0.027$ should have been measured at $\geq 3.7\sigma$ and $\geq 2.3\sigma$, in contrast to the fact that we only obtained upper limits to the EWs.

3. According to the numerical simulations, the WHIM absorbers with $N_{\text{O VII}} \gtrsim 10^{15} \text{ cm}^{-2}$ could sample $> 30\text{--}50\%$ of the O VII-bearing baryons. To systematically survey the 15 QSO sight lines along which the IGM O VI absorbers have been detected, future X-ray telescopes should be able to facilitate the

WHIM study via the X-ray absorption line spectroscopy from background QSOs with fluxes of ~ 0.2 mCrab to find ≥ 10 WHIM systems. It takes impractical long (341 Ms for *Chandra* and 804 Ms for *XMM-Newton*) exposure time for current X-ray telescopes to complete the survey.

4. It would require ~ 11 Ms on-target exposures for future X-ray spectrographs equipped with spectral resolution $R \gtrsim 4000$ and effective area $A \gtrsim 100 \text{ cm}^2$ to finish the survey.

We are grateful to Britton Smith for making his numerical simulation results available to us before publication, and to Charles Danforth for extensive discussion on this work. We thank the anonymous referee for the constructive comments that help to greatly clarify the manuscript. This work is supported by NASA through ADP grant NNX10AE86G, and grant NNX08AC14G to the University of Colorado for data analysis and scientific discoveries related to the Cosmic Origins Spectrograph on the Hubble Space Telescope.

REFERENCES

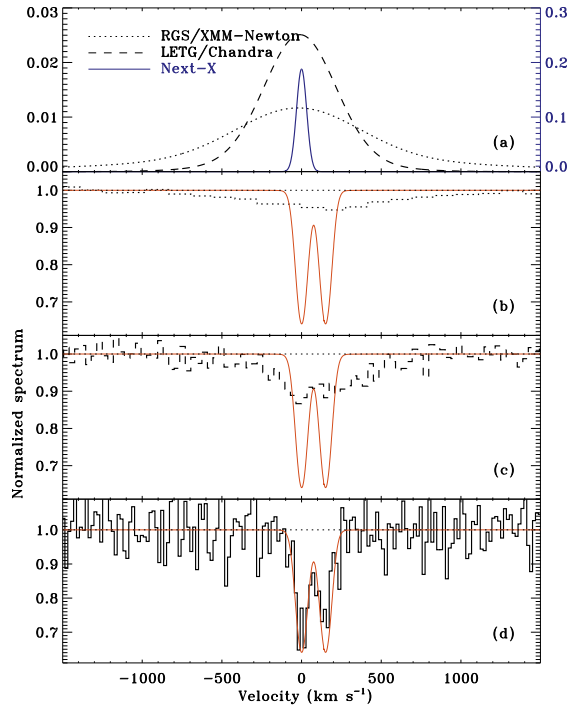


FIG. 9.— Panel (a) shows line spread functions of *XMM-Newton*-RGS (taken from observation 0099280201), *Chandra*-LETG (taken from observation 4148), and a future spectrograph (denoted as “Next-X”) approximated with a Gaussian with FWHM = 75 km s⁻¹. The Next-X uses the right-hand scale. Panels (b)–(d) show the same absorption model (red curves) with two velocity components separated by 150 km s⁻¹ and both characterized as $N_{\text{OVII}} = 10^{15}$ cm⁻² and $b_v = 50$ km s⁻¹ with corresponding simulated absorption spectra (histograms) of *XMM-Newton*-RGS (b), *Chandra*-LETG (c), and Next-X (d) with S/N (per 50 mÅ for *XMM-Newton* and *Chandra* and per 5.4 mÅ for Next-X) = 350, 200, and 30, respectively.

Arnaud, K. A. 1996, *Astronomical Data Analysis Software and Systems V*, A.S.P. Conference Series, Vol. 101, 1996, G. H. Jacoby and J. Barnes, eds., p. 17.

Asplund, M., Grevesse, N., Sauval, A. J., & Scott, P. 2009, *ARA&A*, 47, 481

Bianchi, S., Guainazzi, M., Matt, G., Fonseca Bonilla, N., Ponti, G. 2009, *A&A*, 495, 421

Bregman, J. N. 2007, *ARA&A*, 45, 221

Bregman, J. N., & Lloyd-Davies, E. J. 2007, *ApJ*, 669, 990

Buote, D. A., Zappacosta, L., Fang, T., Humphrey, P. J., Gastaldello, F. & Tagliaferri, G. 2009, *ApJ*, 695, 1351

Burles, S., Nollett, K. M., & Turner, M. S. 2001, *ApJ*, 552, L1

Cagnoni, I., Nicastro, F., Maraschi, L., Treves, A., & Tavecchio, F. 2004, *ApJ*, 603, 449

Canizares, C. R., Schattenburg, M. L. & Smith, H. I. 1986, *SPIE*, 597, 253

Cen, R., & Fang, T. 2006, *ApJ*, 650, 573

Cen, R., & Ostriker, J. P. 2006, *ApJ*, 650, 560

Cen, R., & Ostriker, J. P. 1999, *ApJ*, 514, 1

Chen, X., Weinberg, D. H., Katz, N., & Davé, R. 2003, *ApJ*, 594, 42

Danforth, C. W., & Shull, J. M. 2005, *ApJ*, 624, 555

Danforth, C. W., & Shull, J. M. 2008, *ApJ*, 679, 194

Danforth, C. W., Stocke, J. T., & Shull, J. M. 2010, *ApJ*, 710, 613

Danforth, C. W., Shull, J. M., Rosenberg, J. L., & Stocke, J. T. 2006, *ApJ*, 640, 716

Danforth, C. W., Stocke, J. T., Keeney, B. A., Penton, S. V., Shull, J. M., Yao, Y., & Green, J. C. 2011, *ApJ*, 743, 18

Davé, R., et al. 2001, *ApJ*, 552, 473

Fang, T., McKee, C. F., Canizares, C. R., & Wolfire, M. 2006, *ApJ*, 644, 174

Fang, T., Buote, D. A., Humphrey, P. J., Canizares, C. R., Zappacosta, L., Maiolino, R., Tagliaferri, G., & Gastaldello, F. 2010, *ApJ*, 714, 1715

Fang, T., Marshall, H. L., Lee, J. C., Davis, D. S., & Canizares, C. R. 2002a, *ApJ*, 572, L127

Fang, T., Bryan, G. L., & Canizares, C. R. 2002b, *ApJ*, 564, 604

Fang, T., Canizares, C. R., & Yao, Y. 2007, *ApJ*, 670, 992

Foschini, L., et al. 2006, *A&A*, 453, 829

Fukugita, M., & Peebles, P. J. E. 2004, *ApJ*, 616, 643

Fukugita, M., Hogan, C. J., & Peebles, P. J. E. 1998, *ApJ*, 503, 518

Furlanetto, S. R., Phillips, L. A., & Kamionkowski, M. 2005, *MNRAS*, 359, 295

Galeazzi, M., Gupta, A., Covey, K., & Ursino, E. 2007, *ApJ*, 658, 1081

Gnat, O., & Sternberg, A. 2007, *ApJS*, 168, 213

Juett, A. M., Schulz, N. S., Chakrabarty, D., & Gorczyca, T. W. 2006, *ApJ*, 648, 1066

Kaastra, J. S., Werner, N., den Herder, J. W. A., Paerels, F. B. S., de Plaa, J., Rasmussen, A. P., & de Vries, C. P. 2006, *ApJ*, 652, 189

Komatsu, E., et al. 2011, *ApJS*, 192, 18

Lehner, N., Savage, B. D., Richter, P., Sembach, K. R., Tripp, T. M., & Wakker, B. P. 2007, *ApJ*, 658, 680

Lehner, N., Savage, B. D., Wakker, B. P., Sembach, K. R., & Tripp, T. M. 2006, *ApJS*, 164, 1

Leighly, K. M., Halpern, J. P., Jenkins, E. B., Grupe, D., Choi, J., Prescott, K. B. 2007, *ApJ*, 663, 103

Marshall, H. L., Tennant, A., Grant, C. E., Hitchcock, A. P., O’Dell, S. L., & Plucinsky, P. P. 2004, *SPIE*, 5165, 497

Miller, J. M., Raymond, J., Fabian, A., Steeghs, D., Homan, J., Reynolds, C., van der Klis, M., & Wijnands, R. 2006, *Nature*, 441, 953

Mulchaey, J. S. 2000, *ARA&A*, 38, 289

Narayanan, A., et al. 2011, *ApJ*, 730, 15

Narayanan, A., Wakker, B. P., & Savage, B. D. 2009, *ApJ*, 703, 74

Nicastro, F., et al. 2005, *ApJ*, 629, 700

O’Meara, J. M., Burles, S., Prochaska, J. X., Prochter, G. E., Bernstein, R. A., & Burgess, K. M. 2006, *ApJ*, 649, L61

Oppenheimer, B. D. & Davé, R. 2009, *MNRAS*, 395, 1875

Paerels, F. B. S., & Kahn, S. M. 2003, *ARA&A*, 41, 291

Papadakis, I. E., Brinkmann, W., Page, M. J., Mc Hardy, I., & Uttley, P. 2007, *A&A*, 461, 931

Penton, S. V., Shull, J. M., & Stocke, J. T. 2000, *ApJ*, 544, 150

Penton, S. V., Stocke, J. T., & Shull, J. M. 2004, *ApJS*, 152, 29

Pettini, M., Zych, B. J., Murphy, M. T., Lewis, A., & Steidel, C. C. 2008, *MNRAS*, 391, 1499

Porquet, D., Reeves, J. N., O’Brien, P., & Brinkmann, W. 2004, *A&A*, 422, 85

Prochaska, J. X., Chen, H.-W., Howk, J. C., Weiner, B. J., & Mulchaey, J. 2004, *ApJ*, 617, 718

Protassov, R., van Dyk, D. A., Connors, A., Kashyap, V. L., Siemiginowska, A. 2002, *ApJ*, 571, 545

Rasmussen, A. P., Kahn, S. M., Paerels, F., den Herder, J. W., Kaastra, J., & de Vries, C. 2007, *ApJ*, 656, 129

Rauch, M., et al. 1997, *ApJ*, 489, 7

Reeves, J. N., & Turner, M. J. L. 2000, *MNRAS*, 316, 234

Richter, P., Savage, B. D., Tripp, T. M., & Sembach, K. R. 2006, *A&A*, 451, 767

Savage, B. D., Narayanan, A., Lehner, N., & Wakker, B. P. 2011, *ApJ*, 731, 14

Savage, B. D., Lehner, N., Wakker, B. P., Sembach, K. R., & Tripp, T. M. 2005, *ApJ*, 626, 776

Savage, B. D., et al. 2010, *ApJ*, 719, 1526

Shull, J. M., Penton, S. V., Stocke, J. T., Giroux, M. L., van Gorkom, J. H., Lee, Y. H., & Carilli, C. 1998, *AJ*, 116, 2094

Shull, J. M., Smith, B. D., & Danforth, C. W. 2011, *ApJ*, submitted

Shull, J. M., Tumlinson, J., & Giroux, M. L. 2003, *ApJ*, 594, L107

Smith, B., Hallman, E., Shull, J. M., & O’Shea, B. W. 2012, *ApJ*, in preparation

Softan, A. M., Freyberg, M., Hasinger, G., Miyaji, T., Treyer, M., & Jürmper, J. 1999, *A&A*, 349, 354

Sun, M., Voit, G. M., Donahue, M., Jones, C., Forman, W., & Vikhlinin, A. 2009, *ApJ*, 693, 1142

Tepper-García, T., Richter, P., Schaye, J., Booth, C. M., Dalla Vecchia, C., Theuns, T., & Wiersma, R. P. C., *MNRAS*, 2011, 413, 190

Testa, P., Huenemoerder, D. P., Schulz, N. S., & Ishibashi, K. 2008, *ApJ*, 687, 579

Thom, C., & Chen, H.-W. 2008, *ApJ*, 179, 37

Tripp, T. M., Sembach, K. R., Bowen, D. V., Savage, B. D., Jenkins, E. B., Lehner, N., & Richter, P. 2008, *ApJS*, 177, 39

Tripp, T. M., Savage, B. D., & Jenkins, E. B. 2000, *ApJ*, 534, L1

Ueda, Y., Ishisaki, Y., Takahashi, T., Makishima, K., & Ohashi, T. 2005, *ApJS*, 161, 185

Ursino, E., & Galeazzi, M. 2006, *ApJ*, 652, 1085

Verner, D. A., Verner, E. M., & Ferland, G. J. 1996, *At. Data Nucl. Data Tables*, 64, 1

Verrecchia, F., in’t Zand, J. J. M., Giommi, P., Santolamazza, P., Granata, S., Schuurmans, J. J., & Antonelli, L. A. 2007, *A&A*, 472, 705

Wang, Q. D., Connolly, A., & Brunner, R. 1997, *ApJ*, 487, L13

- Wang, Q. D., et al. 2005, *ApJ*, 635, 386
Weymann, R. J., et al. 1998, *ApJ*, 506, 1
White, N. E., Giommi, P., & Angelini, L. 2000, *yCat*, 9031, 0
Wilkes, B. J., & Elvis, M. 1987, *ApJ*, 323, 243
Williams, R. J., Mulchaey, J. S., Kollmeier, J. A., & Cox, T. J. 2010, *ApJ*, 724, L25
Yao, Y., Shull, J. M., Danforth, C. W., Keeney, B., & Stocke, J. T. 2011, *ApJ*, 730, 143
Yao, Y., & Wang, Q. D. 2005, *ApJ*, 624, 751
Yao, Y., & Wang, Q. D. 2007, *ApJ*, 658, 1088
Yao, Y., Wang, Q. D., Hagihara, T., Mitsuda, K., McCammon, D., & Yamasaki, N. Y. 2009, *ApJ*, 690, 143
Yao, Y., Wang, Q. D., Penton, S. V., Tripp, T. M., Shull, J. M., & Stocke, J. T. 2010, *ApJ*, 716, 1514
Yao, Y., Nowak, M. A., Wang, Q. D., Schulz, N. S., & Canizares, C. R. 2008, *ApJ*, 672, L21
Yao, Y., & Wang, Q. D. 2006, *ApJ*, 641, 930
Zappacosta, L., Nicastro, F., Maiolino, R., Tagliaferri, G., Buote, D. A., Fang, T., Humphrey, P. J., & Gastaldello, F. 2010, *ApJ*, 717, 74